Journal of the Korean Physical Society, Vol. 35, No. 5, November 1999, pp. 393∼398

Bifurcations in a Horizontally Driven Pendulum

Jaeyong JEONG and Sang-Yoon KIM*

Department of Physics, Kangwon National University, Chunchon 200-701

(Received 25 May 1999)

We consider a forced pendulum with a horizontally oscillating suspension point. Bifurcations associated with stability of the symmetric period-1 orbit (SPO), arising from the "unforced" stationary point, are investigated in details by varying the two parameters A (the normalized driving amplitude) and Ω (the normalized natural frequency). We thus obtain the phase diagram showing the bifurcation curves of the SPO in the $\Omega - A$ plane through numerical calculations of the Floquet (stability) multipliers and winding numbers. We note that a specific substructure in the bifurcation set of the SPO recurs in the parameter plane.

I. INTRODUCTION

We consider a horizontally driven pendulum (HDP) whose suspension point undergoes a horizontal periodic oscillation. The system is described by a second-order non-autonomous ordinary differential equation,

$$ml^2\ddot{\theta} + b\dot{\theta} + mgl\sin\theta = ml\omega^2\epsilon\cos\omega t\cos\theta, \qquad (1)$$

where the overdot denotes the differentiation with respect to time, b is a damping coefficient, m is a mass attached to one end of a light thin rod (its mass may be negligible) of length l, θ is the angular displacement measured counterclockwise from the downward vertical, and ϵ and ω are the driving amplitude and frequency of the horizontal oscillation of the suspension point, respectively. Making the normalization $\omega t \to 2\pi t$ and $\theta \to 2\pi x$, we obtain a dimensionless normalized form of Eq. (1),

$$\ddot{x} + 2\pi\beta\Omega\dot{x} + 2\pi\Omega^2\sin 2\pi x = 2\pi A\cos 2\pi t\cos 2\pi x, \qquad (2)$$

where $\omega_0 = \sqrt{g/l}$, $\beta = b/ml^2\omega_0$, $\Omega = \omega_0/\omega$, and $A = \epsilon/l$. This gravitational pendulum has an exact analog in the case of a magnetic pendulum consisting of a permanent magnet placed in a crossed steady and time-varying magnetic field [1]. For the case of the magnetic pendulum, a lower bound on the chaotic regime obtained by the Melnikov method has been confirmed both experimentally and numerically, as in the forced double-well Duffing oscillator [2]. To our knowledge, this is the only work on the HDP.

In contrast with the HDP, the parametrically forced pendulum with a vertically-oscillating suspension point has been extensively studied both theoretically and experimentally [3,4], and thus rich dynamical behaviors have been found. One of its interesting behaviors is a cascade of "resurrections" of the stationary points of the vertically driven pendulum (*i.e.*, the stationary points become stabilized after their instability, destabilize again and so forth *ad infinitum*). One of us (Kim) studied the bifurcations associated with such resurrections in detail [4]. In this paper, we study the bifurcations in the HDP and thus find that the HDP also exhibits interesting bifurcation behaviors, as will be seen below.

For the unforced case with $A = 0$, there exists a stable stationary point with $x = 0$ and $\dot{x} = 0$. However, as A is increased from 0, a stable symmetric period-1 orbit (SPO) arises from the "unforced" stationary point. Here we are particularly interested in the bifurcations associated with the stability of the SPO. By varying the two parameters A and Ω, we make a detailed numerical investigation of bifurcations in the HDP for a fixed value of the normalized damping coefficient β.

This paper is organized as follows. In Sec. II, we discuss bifurcations associated with stability of periodic orbits, using the Floquet theory [5]. The bifurcation behaviors associated with the stability of the SPO are then investigated through numerical calculations of its Floquet (stability) multipliers and winding numbers, characterizing the topological property of the SPO, in Sec. III. We thus obtain the phase diagram showing a periodic recurrence of a specific substructure in the bifurcation set of the SPO, as in other driven oscillators such as the forced Duffing [6], Toda [7], and Morse [8] oscillators. However, the recurrent substructure for the HDP is different from that for the Duffing, Toda, and Morse oscillators. Finally, a summary is given in Sec. IV.

*E-mail: sykim@cc.kangwon.ac.kr

II. STABILITY, BIFURCATIONS, AND WINDING NUMBERS

In this section, we first discuss stability of periodic orbits in the Poincaré map of the HDP, using the Floquet theory [5]. Bifurcations associated with the stability and winding numbers, giving the topological information of the local flow, are then discussed.

The second-order ordinary differential equation (2) is reduced to two first-order ordinary differential equations:

$$\dot{x} = y, \tag{3a}$$

$$\dot{y} = f(x,y,t) = -2\pi\beta\Omega y - 2\pi\Omega^2 \sin 2\pi x + 2\pi A \cos 2\pi t \cos 2\pi x. \tag{3b}$$

These equations have a symmetry S, because the transformation,

$$S : x \to -x,\ y \to -y,\ t \to t + \frac{1}{2}, \tag{4}$$

leaves Eq. (3) invariant. If an orbit $z(t)[\equiv (x(t), y(t))]$ is invariant under S, it is called a symmetric orbit. Otherwise, it is called an asymmetric orbit and has its "conjugate" orbit $Sz(t)$.

The phase space of the HDP is three dimensional with the coordinates x, y, and t. Since the HDP is periodic in t, it is convenient to regard time as a circular coordinate (with mod 1) in the phase space. We then consider the surface of section, the $x-y$ plane at interger times (*i.e.*, $t = m$, m: integer). The phase-space trajectory intersects this plane in a sequence of points. This sequence of points corresponds to a mapping on the plane. This map plot of an initial point z_0 $[= (x_0, y_0)]$ can be conveniently generated by sampling the orbit points z_m at the discrete time $t = m$. We call the transformation $z_m \to z_{m+1}$ the Poincaré map and write $z_{m+1} = P(z_m)$.

The linear stability of a q-periodic orbit of P such that $P^q(z_0) = z_0$ is determined from the linearized-map matrix DP^q of P^q at an orbit point z_0. Here P^q means the q-times iterated map. Using the Floquet theory [5], the matrix DP^q can be obtained by integrating the linearized differential equations for small perturbations as follows.

Let $z^*(t) = z^*(t+q)$ be a solution lying on the closed orbit corresponding to the q-periodic orbit. In order to determine the stability of the closed orbit, we consider an infinitesimal perturbation $\delta z[= (u, v)]$ to the closed orbit. Linearizing Eq. (3) about the closed orbit, we obtain

$$\begin{pmatrix} \dot{u} \\ \dot{v} \end{pmatrix} = J(t) \begin{pmatrix} u \\ v \end{pmatrix}, \quad J(t) = \begin{pmatrix} 0 & 1 \\ f_x(x^*,t) & f_y \end{pmatrix}. \tag{5}$$

Here f_x and f_y denote the partial derivatives of $f(x,y,t)$ in Eq. (3) with respect to the variables x and y, respectively. They are given by

$$f_x(x,t) = -4\pi^2\Omega^2 \cos 2\pi x - 4\pi^2 A \cos 2\pi t \sin 2\pi x,$$
$$f_y = -2\pi\beta\Omega. \tag{6}$$

Note that J is a 2×2 q-periodic matrix. Let $W(t) = (w^1(t), w^2(t))$ be a fundamental solution matrix with $W(0) = I$. Here $w^1(t)$ and $w^2(t)$ are two independent solutions expressed in column vector forms, and I is the 2×2 unit matrix. Then a general solution of the q-periodic system has the following form

$$\begin{pmatrix} u(t) \\ v(t) \end{pmatrix} = W(t) \begin{pmatrix} u(0) \\ v(0) \end{pmatrix}. \tag{7}$$

Substitution of Eq. (7) into Eq. (5) leads to an initial-value problem to determine $W(t)$

$$\dot{W}(t) = J(t)W(t), \quad W(0) = I. \tag{8}$$

It is clear from Eq. (7) that $W(q)$ is just the linearized-map matrix $DP^q(z_0)$. Hence the matrix DP^q can be obtained through integration of Eq. (8) over the period q.

The characteristic equation of the linearized-map matrix $M(\equiv DP^q)$ is

$$\lambda^2 - \mathrm{tr}M\,\lambda + \det M = 0, \tag{9}$$

where $\mathrm{tr}M$ and $\det M$ denote the trace and determinant of M, respectively. The eigenvalues, λ_1 and λ_2, of M are called the Floquet (stability) multipliers. By using the Liouville's formula [9], we obtain the determinant of M ($\det M$),

$$\det M = e^{-2\pi\beta\Omega q}. \tag{10}$$

Consequently, the Poincaré map P becomes a two-dimensional (2D) dissipative map with a constant Jacobian determinant (less than unity).

The pair of Floquet multipliers of a periodic orbit with period q lies either on the circle of radius $e^{-\pi\beta\Omega q}$ or on the real axis in the complex plane. The periodic orbit is stable only when both Floquet multipliers lie inside the unit circle. We first note that they never cross the unit circle, except at the real axis, and hence Hopf bifurcations do not occur. Consequently, a stable periodic orbit can lose its stability when a Floquet multiplier passes through 1 or -1 on the real axis. When a Floquet multiplier decreases through -1, the stable periodic orbit becomes unstable via a period-doubling bifurcation. On the other hand, when a Floquet multiplier increases through 1, it loses its stability via a saddle-node or pitchfork bifurcation. For more details on bifurcations, refer to Ref. 10.

We now discuss the winding number of an orbit, which counts the average number of rotations of neighboring orbits around the given orbit during the time 1 (*i.e.*, one iteration of P). To measure the rotations, we express the linearized equations (5) for the displacements in terms of the polar coordinates $u = r\cos\phi$ and $v = r\sin\phi$,

$$\dot{r} = r[(1 + f_x)\sin\phi\cos\phi + f_y \sin^2\phi],$$
$$\dot{\phi} = -\sin^2\phi + (f_x \cos\phi + f_y \sin\phi)\cos\phi. \tag{11}$$

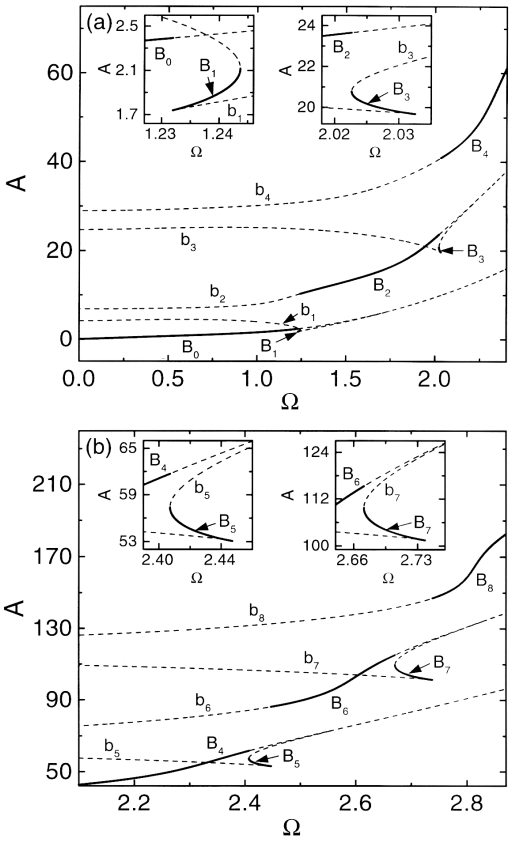

Fig. 1. Phase Diagram showing the bifurcation curves of the SPO for (a) $0 \le \Omega \le 2.4$ and (b) $2.1 \le \Omega \le 2.87$. There exist an infinity of disconnected bifurcation curves B_n $(n = 0, 1, 2, \ldots)$ of the SPO, labelled by its winding number ω. When crossing a solid curve B_n of even order n, the SPO becomes unstable via a pitchfork bifurcation, while it disappears via a saddle-node bifurcation when crossing a solid curve B_n of odd n. Each solid curve B_n also extends over the entire Ω range by joining with the separate parts of the dashed bifurcation curve b_n of another symmetric period-1 orbit born via a saddle-node bifurcation, which is also labelled by its winding number. Note that with increasing Ω, a sequence of bifurcation curves with similar shapes and with increasing winding numbers appears. Enlarged views near the saddle-node bifurcation curves B_n $(n = 1, 3, 5, 7)$ are also given in the insets. For other details, see the text.

The motions of the displacements (r, ϕ) contain all the information about the nearby orbits. Hence we first obtain the Poincaré maps of an initial displacement (r_0, ϕ_0) by sampling the displacements (r_m, ϕ_m) at the discrete time $t = m$ $(m = 1, 2, 3, \ldots)$. Then the average exponential rate of growth of the radius r gives the largest Lyapunov exponent, while the increase in the angle ϕ (normalized by the factor 2π) can be used to define the winding number w,

$$w = \lim_{m \to \infty} \frac{|\phi_m - \phi_0|}{2\pi m}. \qquad (12)$$

For more details on the winding number, refer to Ref. 11.

III. BIFURCATIONS OF THE SPO

In this section, by varying the two parameters A and Ω, we study bifurcations associated with stability of the SPO for a moderately damped case of $\beta = 0.5$. We thus obtain the phase diagram, showing a recurrent structure in the bifurcation set of the SPO.

As explained in Sec. II, the linear stability of a periodic orbit with period q in the Poincaré map P is determined from the linearized-map matrix $M(\equiv DP^q)$ of P^q. The matrix M can be obtained through numerical integration of Eq. (8) over the period q, and then its eigenvalues give the Floquet multipliers of the periodic orbit. In such a way, we determine the stability of the SPO in the $\Omega - A$ plane through numerical calculations of its Floquet multipliers, and then we investigate in detail the bifurcation behaviors of the SPO at the stability boundary curves. The winding number ω of the SPO at each bifurcation curve is also obtained through numerical computation of Eq. (12) to characterize its topological property. It is thus found that there exist an infinity of disconnected bifurcation curves B_n $(n = 0, 1, 2, \ldots)$ of the SPO, labelled by its winding numbers ω, some of which are denoted by heavy solid curves in the phase diagram shown in Fig. 1.

The bifurcation behaviors of the SPO depend on whether the order n of the bifurcation curve B_n is even or odd. When crossing a bifurcation curve B_n of even order n, the SPO becomes unstable via a pitchfork bifurcation, while it disappears via a saddle-node bifurcation when crossing a bifurcation curve B_n of odd order n. It is also found that each such bifurcation curve B_n of the SPO extends over the whole Ω range by joining with the separate parts of a bifurcation curve, denoted by dashed curves in Fig. 1, of another symmetric period-1 orbit born via a saddle-node bifurcation. Hereafter, each dashed curve, joining with the solid curve B_n, will be represented by b_n $(n = 0, 1, 2, \ldots)$. We first note that, when the bifurcation curve b_n of odd order n is crossed, a saddle-node bifurcation occurs, which results in the birth of a pair of stable and unstable symmetric period-1 orbits with the winding number $\omega = n$. As shown in Fig. 1, there exist two separate b_n's for each odd n. The "left" ("right") b_n connects with the right (left) end point of the solid curve B_n. The stable symmetric period-1 orbit born at the left (right) b_n of odd order n becomes unstable via a pitchfork bifurcation at the left (right) dashed curve b_{n+1} (b_{n-1}) of even order $n + 1$ $(n - 1)$, where the winding number of the symmetric period-1 orbit becomes $n + 1$ $(n - 1)$. The dashed curve b_n of even order n also connects with the solid curve B_n.

From now on, we present concrete examples of the bifurcations explained above. We first consider the bifurcations associated with the stability of the SPO. The bifurcation diagrams and the phase-portrait plots are also given for clear presentation of the bifurcations. As an

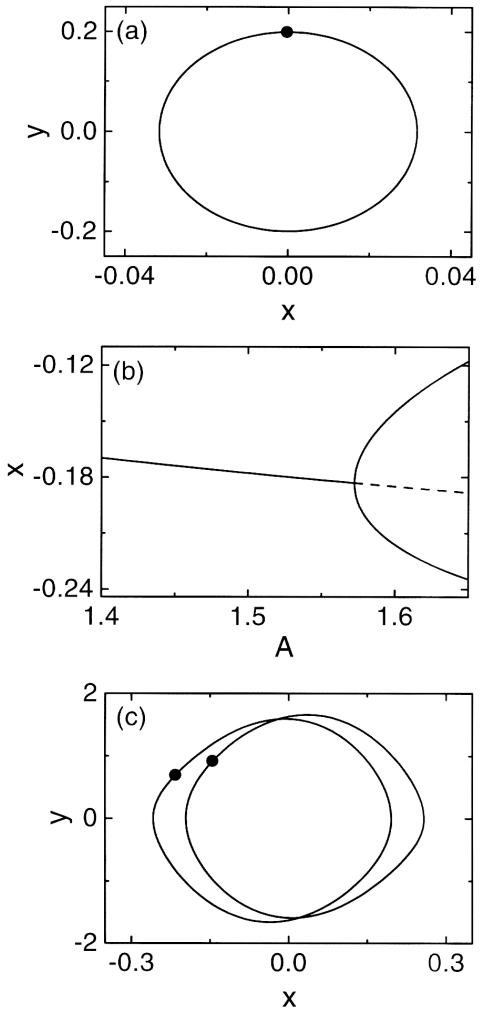

Fig. 2. Phase portraits and a bifurcation diagram for $\Omega = 1.0$. (a) For $A = 0.1$ the phase flow of the SPO, arising from the "unforced" stationary point, is denoted by a solid curve, and its Poincaré map is represented by a solid circle. (b) A bifurcation diagram (plot of x vs. A) near the pitchfork bifurcation point $A_b (= 1.572\,491\cdots)$. Here the solid curve denotes a stable periodic orbit, while the dashed curve represent an unstable periodic orbit. (c) For $A = 1.6$ the phase flows of a conjugate pair of asymmetric period-1 orbits, born by the pitchfork bifurcations, are denoted by the solid curves, while their Poincaré maps are represented by the solid circles.

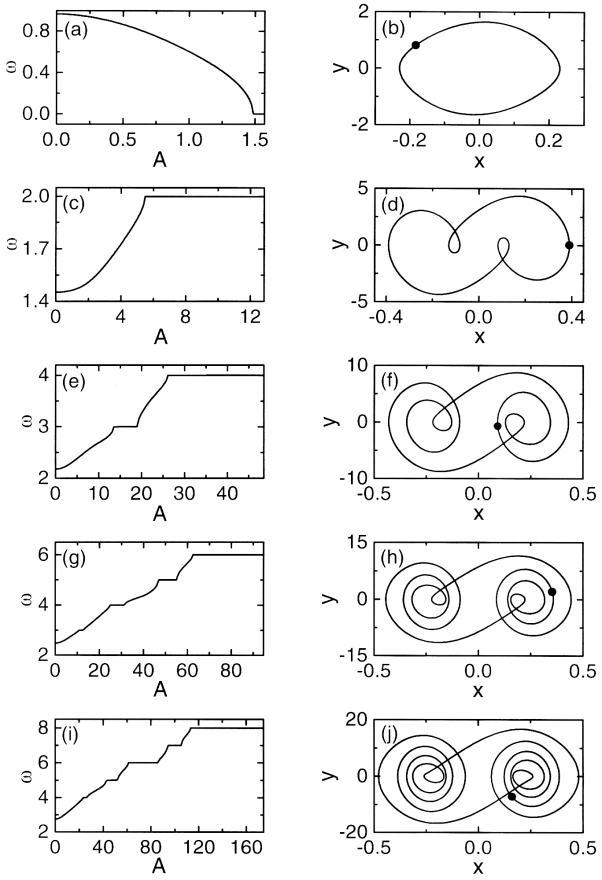

Fig. 3. Plots of the winding number of the SPO, ω, vs. A in the range between $A = 0$ and the pitchfork bifurcation point A_b and the phase portraits of the SPO at the pitchfork bifurcation points A_b for (a) and (b) $\Omega = 1.0$, (c) and (d) $\Omega = 1.5$, (e) and (f) $\Omega = 2.25$, (g) and (h) $\Omega = 2.56$, and (i) and (j) $\Omega = 2.86$. Here the phase flows are denoted by solid curves, while the Poincaré maps are represented by solid circles.

example, we consider the case of $\Omega = 1.0$. For $A = 0$, there exists a stationary point with $(x, \dot{x}) = (0, 0)$. However, as A is increased from 0, a stable SPO arises from the unforced stationary point, and its phase portrait for $A = 0.1$ is shown in Fig. 2(a). This SPO becomes unstable via a pitchfork bifurcation when the bifurcation curve B_0 is crossed at its bifurcation point A_b $(= 1.572\,491\cdots)$ [see Fig. 1(a)]. The bifurcation diagram near this bifurcation is also shown in Fig. 2(b). Through the symmetry-breaking pitchfork bifurcation, a conjugate pair of asymmetric period-1 orbits appears, and their phase portraits for $A = 1.6$ are shown in Fig. 2(c). As in the case of B_0, when crossing the curves B_n of even order n, the SPO loses its stability via a pitchfork bifurcation. However, the winding number ω of the SPO at the curve B_n increases with the order n. As an example, we take some representative values $\Omega = 1.0$, 1.5, 2.25, 2.56, and 2.84 for the bifurcation curves B_n with $n = 0, 2, 4, 6$ and 8, respectively. The plots of ω vs. A for representative values of Ω are given in the left column of Fig. 3. Note that the winding numbers near the bifurcation points take even-interger values of 0, 2, 4, 6, and 8, respectively. That is, the order n of the bifurcation curve is just the winding number ω of the SPO (*i.e.*, $\omega = n$). The phase portraits of the SPO at the bifurcation points are given in the right column of Fig. 3. Note that the SPO at the curve B_n has an increasing number of loops, because the winding number increases with n.

Unlike the above case, the SPO disappears via a

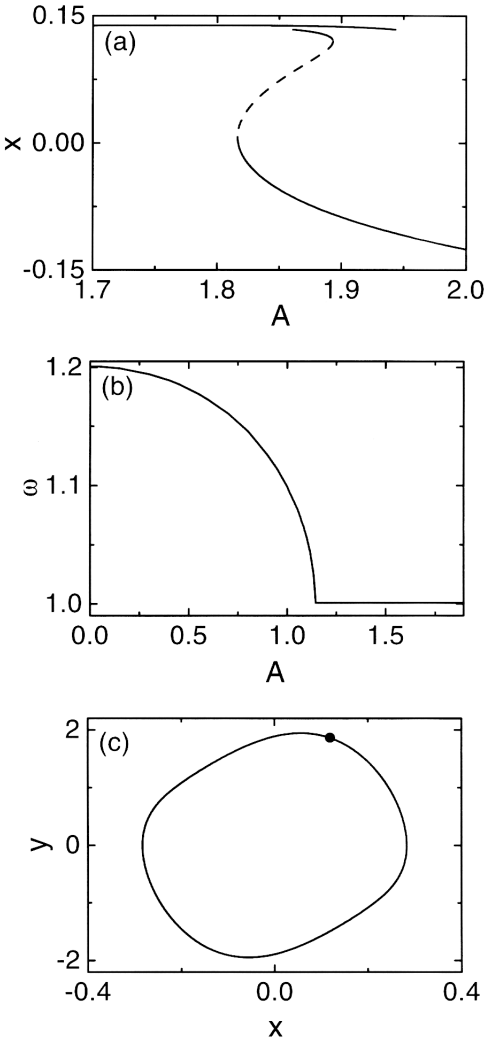

Fig. 4. (a) Bifurcation diagram near the saddle-node bifurcation for $\Omega = 1, 24$. Here the solid curve denotes a stable periodic orbit, while the dashed curve represents an unstable periodic orbit. (b) Plot of the winding number of the SPO ω vs. A in the range between $A = 0$ and the saddle-node bifurcation point A_b. (c) Phase flow (Poincaré map) of the SPO at the saddle-node bifurcation point A_b ($= 1.893\,191\cdots$) is denoted by a solid curve (circle).

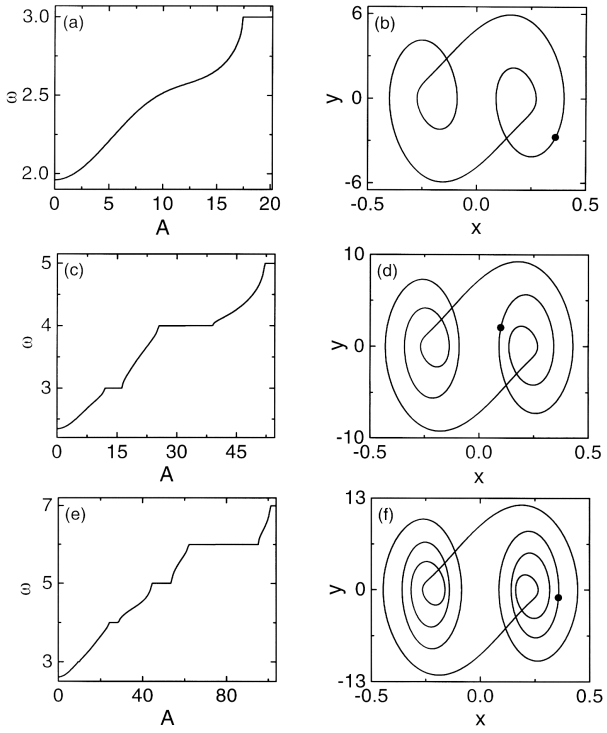

Fig. 5. Plots of the winding number of the SPO ω vs. A in the range between $A = 0$ and the saddle-node bifurcation point A_b and the phase portraits of the SPO at the saddle-node bifurcation points A_b for (a) and (b) $\Omega = 2.025$, (c) and (d) $\Omega = 2.42$, and (e) and (f) $\Omega = 2.70$. Here the phase flows are denoted by solid curves, while the Poincaré maps are represented by solid circles.

saddle-node bifurcation when crossing a bifurcation curve B_n of odd n. As an example, we consider the case of $\Omega = 1.24$. The bifurcation diagram near the saddle-node bifurcation is shown in Fig. 4(a). When the curve B_1 is crossed at the bifurcation point A_b ($= 1.893\,191\cdots$), the SPO disappears via a saddle-node bifurcation by absorbing an unstable period-1 orbit born at the dashed saddle-node bifurcation curve b_1 just below the curve B_1 [see the left inset in Fig. 1(a)]. After the disappearance of the SPO, the state of the system jumps to another stable symmetric period-1 orbit born via a saddle-node bifurcation at the curve b_1. The plot of ω vs. A and the phase portrait at the bifurcation point A_b are also given in Figs. 4(b) and 4(c), respectively. Note that the winding number ω takes the value of 1 near the bifurcation point. Such saddle-node bifurcations occur when crossing the bifurcation curves B_n of odd order n. However, the winding number ω of the SPO increases with n, like the case of even-order n. As an example, we take some representative values $\Omega = 2.025$, 2.42, and 2.70 for the bifurcation curves B_n with $n = 3, 5$, and 7, respectively. The left column of Fig. 5 shows the plots of ω vs. A for the representative values of Ω. The winding numbers near the bifurcation points take odd-interger values of 3, 5, and 7, respectively. The phase portraits of the SPO at the bifurcation points are also shown in the right column of Fig. 5. Note also that the SPO at the curve B_n has an increasing number of loops with n.

As mentioned above, each curve B_n of the SPO joins with the separate parts of the dashed bifurcation curves b_n of another symmetric period-1 orbit born via a saddle-node bifurcation. When the curve b_n of odd order n is crossed, a saddle-node bifurcation takes place, which leads to the birth of a pair of stable and unstable symmetric period-1 orbits with winding numbers n. As A is increased, each newly-born stable period-1 orbit becomes unstable via a pitchfork bifurcation at the dashed

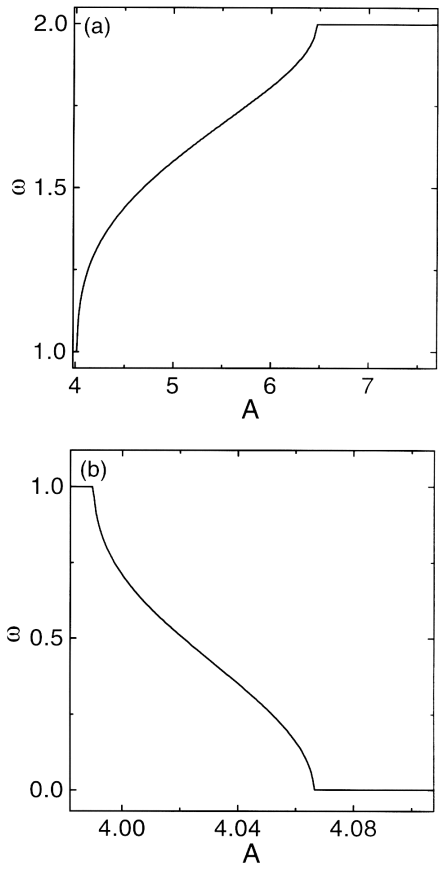

Fig. 6. Plots of the winding number ω vs. A for the symmetric period-1 orbit born at the dashed saddle-node bifurcation curve b_1 in case of (a) $\Omega = 1.0$ and (b) $\Omega = 1.5$.

curve b_n of even order. However, the change in the winding number of the symmetric period-1 orbit depends on whether it is born at the left or right dashed curve b_n. As an example, we take two representative values, $\Omega = 1.0$ and 1.5, for the left and right parts of the curve b_1, respectively. Figure 6 shows the plots of ω vs. A for the representative values of Ω. The winding number for the case of $\Omega = 1.0$ increases by 1, while it decreases by 1 for $\Omega = 1.5$. In such a way, the symmetric period-1 orbit born at the left (right) dashed curve b_n of odd n loses its stability via pitchfork bifurcation at the left (right) dashed curve b_{n+1} (b_{n-1}) of even order $n+1$ ($n-1$).

Finally, we note that the bifurcation set in Fig. 1 consists of the recurrence of a specific substructure of the bifurcation curves. To show this recurrence, we denote the connected bifurcation curve of B_n and b_n by L_n (*i.e.*, $L_n = B_n \cup b_n$). The first nine curves L_n's ($n = 0, 1, \ldots, 8$) are shown in Fig. 1. As an example, compare the structure of $L_4 \cup L_5$ and $L_6 \cup L_7$ in Fig. 1(b) with that of $L_2 \cup L_3$ in Fig. 1(a). Then one can easily see that each pair of the bifurcation curves has a similar structure. It is thus expected that higher-order pairs of bifurcation curves $L_n \cup L_{n+1}$ ($n = 8, 10, \ldots$) with similar structures will appear successively with increasing Ω.

IV. SUMMARY

A detailed investigation of the bifurcations, associated with the stability of the SPO, has been made through numerical calculations of the Floquet multipliers and winding numbers. We have thus obtained the phase diagram, showing a recurrent structure in the bifurcation set of the SPO. Finally, note also that recurrence of a substructure in the bifurcation set occurs in other driven oscillators such as the forced Duffing, Toda and Morse oscillators [6–8]. However, the repeating substructure varies depending on the oscillator.

ACKNOWLEDGMENTS

This work was supported by Biomedlab Inc. and by the Korea Research Foundation under Project No. 1998-015-D00065.

REFERENCES

[1] F. C. Moon, J. Cusumano and P. J. Holmes, Physica **D24**, 383 (1987).
[2] P. J. Holmes, Philos. Trans. R. Soc. London, Ser. **A292**, 419 (1979); F. C. Moon and P. J. Holmes, J. Sound Vib. **65**, 275 (1979).
[3] J. B. McLaughlin, J. Stat. Phys. **24**, 375 (1981); B. P. Koch, R. W. Leven, B. Pompe and C. Wilke, Phys. Lett. **A96**, 219 (1983); P. L. Kapitza, in *Collected Papers of P. L. Kapitza*, edited by D. Ter Haar (Pergamon, London, 1965), p. 714; H. J. T. Smith and J. A. Blackburn, Am. J. Phys. **60**, 909 (1992).
[4] S.-Y. Kim and K. Lee, Phys. Rev. **E53**, 1579 (1996); S.-Y. Kim, S.-H. Shin, J. Yi and C.-W. Jang, Phys. Rev. **E56**, 6613 (1997); S.-Y. Kim and B. Hu, Phys. Rev. **E58**, 3028 (1998).
[5] S. Lefschetz, *Differential Equations: Geometric Theory* (Dover, New York, 1977), Sec. 3.5.
[6] U. Parlitz and W. Lauterborn, Phys. Lett. **A107**, 351 (1985).
[7] T. Kurz and W. Lauterborn, Phys. Rev. **A37**, 1029 (1988).
[8] W. Knop and W. Lauterborn, J. Chem. Phys. **93**, 3950 (1990).
[9] V. I. Arnold, *Ordinary Differential Equations* (MIT Press, Cambridge, 1973), p. 114.
[10] J. Guckenheimer and P. Holmes, *Nonlinear Oscillations, Dynamical Systems, and Bifurcations of Vector Fields* (Springer-Verlag, New York, 1983), Sec. 3.5.
[11] U. Parlitz, Int. J. Bifurcation and Chaos **3**, 703 (1993).